Available online at www.sciencedirect.com
SCIENCE DIRECT
Journal of Organometallic Chemistry 691 (2006) 2810–2820
Journal of Organometallic Chemistry
www.elsevier.com/locate/jorganchem

Role of titanium oxidation states in polymerization activity of Ziegler–Natta catalyst: A density functional study

Sumit Bhaduri [a], Sami Mukhopadhyay [b,*], Sudhir A. Kulkarni [b]

[a] *Reliance Industries Limited, Swastik Mill Compound, V.N. Purav Marg, Chembur, Mumbai 400 071, India*
[b] *VLife Sciences Technologies Private Limited, Research and Development, 1 – Akshay, #50, Anand Park, Aundh, Pune 411 007, India*

Received 7 November 2005; received in revised form 15 February 2006; accepted 15 February 2006
Available online 6 March 2006

Abstract

The role of titanium oxidation states in olefin polymerization activity for Ziegler–Natta (ZN) catalyst has been investigated using density functional calculations at B3LYP/LANL2DZ as well as extended LANL2DZ basis that includes diffuse and polarization functions for C, H and Cl. Using the simple $[TiCl_2CH_3]^n$ ($n = +1, 0, -1$) model catalyst systems, we could rationalize some of the well-known experimental facts with varying Ti oxidation states (+4, +3, +2) in the real ZN systems. Firstly, irrespective of Ti oxidation states, the activation barriers (E_{act}) for ethylene and *syn* propylene insertion in Ti–CH_3 bond are comparable in accordance with experimental and modeling studies. Secondly, it was observed that Ti(IV) catalyst has the lowest E_{act} which progressively increase in the order Ti(IV) < Ti(III) < Ti(II) high spin < Ti(II) low spin catalysts in line with experimental and several modeling results. The effect of solvation on olefin insertion barriers are seen more prominent in case of Ti(IV) systems compared to other oxidation states.

Keywords: Density functional; Ziegler–Natta catalyst; Titanium oxidation states; Activation barriers; Olefin polymerization activity; Solvation

1. Introduction

The Ziegler–Natta (ZN) catalytic system is more than 40 years old. However, more than 90% of the commercial manufacture of polyethylene and polypropylene is still based on modifications and improvements of the original ZN system [1–3]. Apart from their immense technological importance, these catalysts also pose some fundamental questions that are yet to be fully answered. In our earlier publications we provided DFT based explanations for the remarkable difference in the reactivities of ethylene and propylene towards titanium haloalkoxy, alkoxy and non-alkoxy complexes [4,5]. We have also studied the role of electron donors in propylene polymerization [6].

Another fundamental question deals with the assignment of oxidation states to the titanium ions at the active sites. The treatment of $TiCl_4$ with alkyl aluminum is expected and known to lead to the generation of titanium species of lower oxidation states. A variety of techniques such as potentiometric, polarographic, and redox titration have been reported for determining the oxidation states of titanium species present in the catalyst [7–9]. Data based on ESR experiments have also been used [10,11]. However, none of these techniques can differentiate between the bulk and the surface titanium ions.

More recently, Somorjai and co-workers have prepared model catalysts such as a thin film of $TiCl_x/MgCl_2$ deposited on a polycrystalline gold foil, or electron beam-induced deposition of $TiCl_4$ on a gold substrate. These catalysts have been studied by ESCA and related techniques and Ti^{4+}, Ti^{3+}, and Ti^{2+} ions have been identified on the surface [12–14]. Computational studies on probable active sites in ZN catalytic systems and their single site analogues have also been reported [15–17]. Thus, for both monomeric

* Corresponding author. Tel.: +91 20 2588 6737; fax:+91 20 2588 4752.
E-mail addresses: sumit_bhaduri@ril.com (S. Bhaduri), samim@vlifesciences.com (S. Mukhopadhyay), sudhirk@vlifesciences.com (S.A. Kulkarni).

0022-328X/$ - see front matter © 2006 Elsevier B.V. All rights reserved.
doi:10.1016/j.jorganchem.2006.02.019

$TiCl_4$ and $TiCl_3$, coordination on the (1 1 0) $MgCl_2$ face has been found to be favored relative to coordination on the (1 0 0) face [15]. However, while both Ti(IV) and Ti(III) species can bind as stable adducts, for simple adducts Ti(IV) is considered to be the dominant catalytic species [16]. For a constrained geometry catalyst, Fan et al. have also shown that the activation energies of ethylene insertion into the Ti–C bond, are comparable for Ti(IV) and Ti(III) species [17a].

From all these reports it is clear, that more work is required for a definitive answer regarding the oxidation state(s) of titanium at the active sites of ZN catalysts. The work reported in this paper was undertaken from such a perspective. Here, we report comparative results of DFT calculations on model ZN catalysts in the oxidation states of +4, +3 and +2. We have investigated the insertion of ethylene and propylene in the Ti–CH_3 bond for all these oxidation states. Our results show that for both the alkenes the activation barrier for Ti(IV) is substantially less than that of Ti(III) or Ti(II).

2. Methodology

The model active catalysts (having one vacant site as suggested by Cossee, [18]) selected for this work are $[TiCl_2CH_3]^+$, $[TiCl_2CH_3]$, $[TiCl_2CH_3]^{-1}$ (high spin) and $[TiCl_2CH_3]^{-1}$ (low spin) with the corresponding +4, +3, +2 oxidation states for titanium. All the geometries have been obtained using hybrid density functional method B3LYP [19] (three parameter Becke's exchange energy functional along with correlation functional due to Lee, Yang and Parr). The LANL2DZ basis set which includes a double zeta valence basis set (8s5p5d)/[3s3p2d] for Ti with the Hay and Wadt ECP replacing core electrons up to 2p and Huzinaga–Dunning (D95) double zeta basis set for all other atoms has been used throughout the calculations. In order to verify our computational results at level of higher basis set, we have also used the extended basis set including diffuse and polarization functions to LANL2DZ basis for C, H and Cl atoms and will be designated as LANL2DZ* basis herein after [20a].

The vibrational frequencies and zero point energies (ZPE) of all the stationary points have been obtained on the potential energy surface (PES) of ethylene and propylene polymerization for the catalysts described above at both LANL2DZ and LANL2DZ* levels. Single point solvent (toluene) corrected relative energies (kcal/mol) for all the stationary points at LANL2DZ level have also been obtained using CPCM method [20b]. In this method, a PCM (polarized continuum model) calculation is performed using the polarizable conductor calculation model (CPCM) [20b] in presence of solvent. The polarized continuum (overlapping spheres) model (PCM) of Tomasi and co-workers performs a PCM reaction field calculation (SCRF) using the polarizable dielectric model [20c,20d,20e]. The solvent toluene has been selected since it is experimentally the most widely used solvent in these systems. All our calculations have been performed using the program GAUSSIAN 98 [21].

3. Results and discussion

The oxidation state of the metal in the active catalytic species is an important factor for determining the olefin polymerization activity [22]. In the real Ti catalyzed Ziegler–Natta polymerization, Ti exists in several oxidation states of +2, +3, +4 [15–17,23]. Our studies are primarily on the effect of variation of metal oxidation states on Ziegler–Natta catalyst activity and to investigate which Ti oxidation states lead to most promising olefin polymerization activities. This involved studying the olefin insertion step in Ti-alkyl bond as per the Cossee mechanism [18] at a molecular level with different Ti oxidation states.

The optimized structures of all reactants viz. active catalysts and olefins at B3LYP/LANL2DZ level are displayed in Fig. 1. Their corresponding structures at B3LYP/LANL2DZ* level are all similar with an increase of Ti–C(Me) bond lengths, a decrease of Ti–Cl bond lengths but the overall trends of variation of these parameters

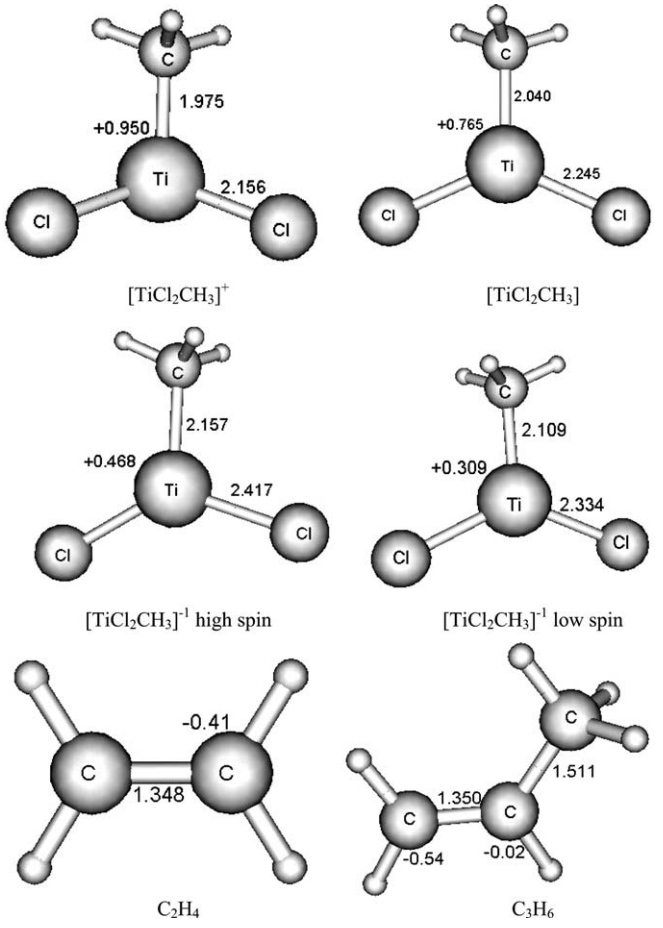

Fig. 1. Geometrical parameters and Mulliken charges for optimized geometries of active catalysts and olefins at B3LYP/LANL2DZ level. Bond lengths are in Å. All the structures have been visualized by using MDS 2.0 molecular modeling software [27].

remain the same as with the LANL2DZ level of calculation (cf. Table 2). Also, the C=C bonds in free ethylene and propylene gets reduced by 0.008 Å on moving to the higher basis set (cf. Table 2). The zero point energy (ZPE) corrected relative energies (kcal/mol) of stationary points on the PES of ethylene and propylene polymerization using $[TiCl_2CH_3]^n$ ($n = +1, 0, -1$) active catalysts corresponding to Ti oxidation states of +4, +3, +2 at B3LYP/LANL2DZ level are reported in Table 1. The corresponding relative energies (kcal/mol) computed at B3LYP/LANL2DZ* level are shown in parentheses (cf. Table 1). The Mulliken charges on Ti in the active catalysts on moving from Ti(IV) to Ti(II) (high and low spins) progressively decrease from +0.950 (Ti(IV)) to +0.765 (Ti(III)) to +0.468 (Ti(II) high spin) to +0.309 (Ti(II) low spin), respectively (cf. Fig. 1), at B3LYP/LANL2DZ level. At B3LYP/LANL2DZ* level, the Mulliken charges on Ti vary from +1.109 (Ti(IV)) to +0.954 (Ti(III)) to +0.702 (Ti(II) high spin) to +0.448 (Ti(II) low spin), respectively, indicating similar trend at both levels of calculations. This is expected due to addition of d electrons to the metal. The important bond lengths (in Å) in active catalysts, olefins and complexes at both levels of calculation are listed in Table 2.

The optimized geometries of stationary points viz. olefin complexes, transition states and products observed on the PES of olefin (ethylene and *syn* propylene as representative examples) insertion in the active catalysts $[TiCl_2CH_3]^+$, $[TiCl_2CH_3]$ and $[TiCl_2CH_3]^{-1}$ (high and low spins) at B3LYP/LANL2DZ level are displayed in Figs. 2–4, respectively. It is observed once again that the overall trends in structural parameters throughout the complexes, TSs and products remain the same at both levels of calculation with the only exception of *syn* propylene complex of Ti(IV) active catalyst, $[TiCl_2CH_3]^+$. This has been discussed in the following sections. The relative energy profiles for ethylene and *syn* propylene insertion into solvated and unsolvated $[TiCl_2CH_3]^+$ at B3LYP/LANL2DZ level are displayed in Figs. 5 and 6, respectively.

Titanium is in distorted tetrahedral environment in all the complexes and TSs (cf. Figs. 2 and 3). The meaning of *syn* and *anti* terminology used throughout this work refers to the relative orientations of the methyl group of propylene with respect to the Ti–CH_3 bond. If both the methyl groups are on the same side then the structure is called *syn*-, otherwise it is referred to as *anti*-. It may be noted that the insertion of propylene in the Ti-alkyl bond in the *syn*- and *anti*-structures leads to the formation of anti-Markovnikov (Ti bonded to unsubstituted or less branched carbon) and Markovnikov products, respectively.

3.1. Structure and bonding aspects

We observe that the Ti–ligand bond distances in the active catalysts get reduced as we move from Ti(II) to Ti(III) and Ti(IV) systems as shown in Table 2. In the active catalysts, the reduction of Ti–CH_3 bond lengths is from Ti(II) high spin to Ti(III) by 0.117 Å and from Ti(III) to Ti(IV) by 0.065 Å at B3LYP/LANL2DZ level and similar reduction values of 0.113 Å and 0.066 Å, respectively, for these at B3LYP/LANL2DZ* level. Similarly for the Ti–Cl bond lengths in active catalysts, the reduction is from Ti(II) high spin to Ti(III) by 0.172 Å and from Ti(III) to Ti(IV) by 0.089 Å at B3LYP/LANL2DZ and similar reduction values of 0.179 and 0.095 Å, respectively, for these at B3LYP/LANL2DZ* level. This may be attributed

Table 1
Zero point energy (ZPE) corrected relative energies (kcal/mol) of stationary points on the PES of ethylene and propylene polymerization using $[TiCl_2CH_3]^n$ ($n = +1, 0, -1$) catalyst at B3LYP/LANL2DZ level[a] and B3LYP/LANL2DZ* level[b] (values in parentheses)

Active catalyst	Olefin	*E*(Complex)	*E*(TS)	E_{act}[c]	*E*(Product)
$[TiCl_2CH_3]^+$	C_2H_4	−37.98 (−35.01)	−29.92 (−29.33)	8.06 (5.73)	−42.49 (−42.27)
	C_3H_6 (Syn)	−40.99 (−41.21)[d]	−33.84 (−32.65)	7.15 (8.56)	−42.05 (−41.96)
	C_3H_6 (Anti)	−48.28 (−43.73)	−30.41 (−29.52)	17.87 (14.21)	−43.66 (−43.62)
$[TiCl_2CH_3]$	C_2H_4	−12.35 (−12.13)	3.92 (3.06)	16.27 (15.19)	−16.59 (−18.04)
	C_3H_6 (Syn)	−12.58 (−12.07)	5.68 (4.65)	18.26 (16.72)	−13.21 (−5.38)
	C_3H_6 (Anti)	−13.63 (−12.97)	7.84 (6.64)	21.47 (19.61)	−13.28 (−7.78)
$[TiCl_2CH_3]^{-1}$ high spin	C_2H_4	−11.90 (−11.88)	17.33 (16.25)	29.23 (28.13)	−14.74 (−16.55)
	C_3H_6 (Syn)	−9.28 (−9.69)	20.83 (18.73)	30.11 (28.42)	−12.36 (−14.67)
	C_3H_6 (Anti)	−9.88 (−10.03)	22.50 (20.79)	32.38 (30.82)	−9.51 (−11.98)
$[TiCl_2CH_3]^{-1}$ low spin	C_2H_4	−36.33 (−35.87)	25.03 (21.38)	61.36 (57.25)	−14.88 (−17.02)
	C_3H_6 (Syn)	−31.91 (−32.30)	28.96 (24.77)	60.87 (57.07)	−12.51 (−15.22)
	C_3H_6 (Anti)	−33.20 (−33.38)	29.26 (24.81)	62.46 (58.19)	−7.81 (−10.90)

[a] Total ZPE corrected energies (electronic + ZPE in au) calculated at B3LYP/LANL2DZ level of active catalysts and olefins are: $[TiCl_2CH_3]^+ = -127.647569$; $[TiCl_2CH_3] = -127.974497$; $[TiCl_2CH_3]^{-1}$ high spin $= -128.045275$; $[TiCl_2CH_3]^{-1}$ low spin $= -128.024322$; $C_2H_4 = -78.526874$; $C_3H_6 = -117.811103$.

[b] Total ZPE corrected energies (electronic + ZPE in au) calculated at B3LYP/LANL2DZ* level (LANL2DZ* = LANL2DZ + diffuse and polarization functions for C, Cl, H) of active catalysts and olefins are: $[TiCl_2CH_3]^+ = -127.687347$; $[TiCl_2CH_3] = -128.004143$; $[TiCl_2CH_3]^{-1}$ high spin $= -128.076918$; $[TiCl_2CH_3]^{-1}$ low spin $= -128.054357$; $C_2H_4 = -78.548846$; $C_3H_6 = -117.844656$.

[c] E_{act} is insertion barrier in kcal/mol.

[d] This structure is the intermediate as discussed in the text.

Table 2
Important bond lengths (in Å) for optimized structures of active catalysts, complexes and olefin at B3LYP/LANL2DZ level and B3LYP/LANL2DZ* level (values in parentheses)

Active catalyst	Bond lengths (Å) (active catalyst)	Olefin	Bond lengths (Å) (Complex)
$[TiCl_2CH_3]^+$Ti(IV)	Ti–Cl 2.156 (2.122) Ti–C(CH_3) 1.975 (1.985)	C_2H_4	Ti–C(et) 2.302 (2.331) Ti–C(et) 2.855 (2.772) C=C (‖)[a] 1.373 (1.361) Ti–C(CH_3) 1.984 (1.997)
		C_3H_6 (Syn)	Ti–C(pp) 2.336 (2.959)[b] Ti–C(pp) 2.732 (2.276)[b] C=C (‖) 1.374 (1.374)[b] Ti–C(CH_3) 1.994 (2.001)[b]
		C_3H_6 (Anti)	Ti–C(pp) 2.234 (2.259) Ti–C(pp) 2.929 (2.840) C=C (‖) 1.390 (1.377) Ti–C(CH_3) 1.987 (1.999)
$[TiCl_2CH_3]$Ti(III)	Ti–Cl 2.245 (2.217) Ti–C(CH_3) 2.040 (2.051)	C_2H_4	Ti–C(et) 2.376 (2.349) Ti–C(et) 2.413 (2.386) C=C (∼⊥)[a] 1.382 (1.372) Ti–C(CH_3) 2.045 (2.058)
		C_3H_6 (Syn)	Ti–C(pp) 2.375 (2.351) Ti–C(pp) 2.529 (2.480) C=C(∼‖) 1.380 (1.372) Ti–C(CH_3) 2.064 (2.073)
		C_3H_6 (Anti)	Ti–C(pp) 2.370 (2.351) Ti–C(pp) 2.490 (2.444) C=C(between ‖ and ⊥) 1.382 (1.373) Ti–C(CH_3) 2.047 (2.058)
$[TiCl_2CH_3]^{-1}$Ti(II) high spin	Ti–Cl 2.417 (2.396) Ti–C(CH_3) 2.157 (2.164)	C_2H_4	Ti–C(et) 2.364 (2.344) Ti–C(et) 2.376 (2.359) C=C (⊥) 1.402 (1.389) Ti–C(CH_3) 2.140 (2.151)
		C_3H_6 (Syn)	Ti–C(pp) 2.404 (2.421) Ti–C(pp) 2.403 (2.334) C=C(∼‖) 1.398 (1.387) Ti–C(CH_3) 2.153 (2.157)
		C_3H_6 (Anti)	Ti–C(pp) 2.383 (2.365) Ti–C(pp) 2.400 (2.379) C=C(∼⊥) 1.400 (1.388) Ti–C(CH_3) 2.144 (2.152)
$[TiCl_2CH_3]^{-1}$Ti(II) low spin	Ti–Cl 2.334 (2.315) Ti–C(CH_3) 2.109 (2.116)	C_2H_4	Ti–C(et) 2.079 (2.080) Ti–C(et) 2.113 (2.116) C=C(∼⊥) 1.474 (1.459) Ti–C(CH_3) 2.095 (2.106)
		C_3H_6 (Syn)	Ti–C(pp) 2.082 (2.084) Ti–C(pp) 2.125 (2.125) C=C(∼⊥) 1.473 (1.459) Ti–C(CH_3) 2.094 (2.103)
		C_3H_6 (Anti)	Ti–C(pp) 2.114 (2.116) Ti–C(pp) 2.084 (2.086) C=C(∼⊥) 1.474 (1.460) Ti–C(CH_3) 2.095 (2.105)

[a] ‖, ⊥ means C=C bond of ethylene(et) or propylene(pp) is parallel, perpendicular to Ti–C(CH_3), respectively. C=C (ethylene) 1.348 Å (1.340 Å); C=C (propylene) 1.350 Å (1.342 Å).
[b] The values correspond to intermediate structure as discussed in the text.

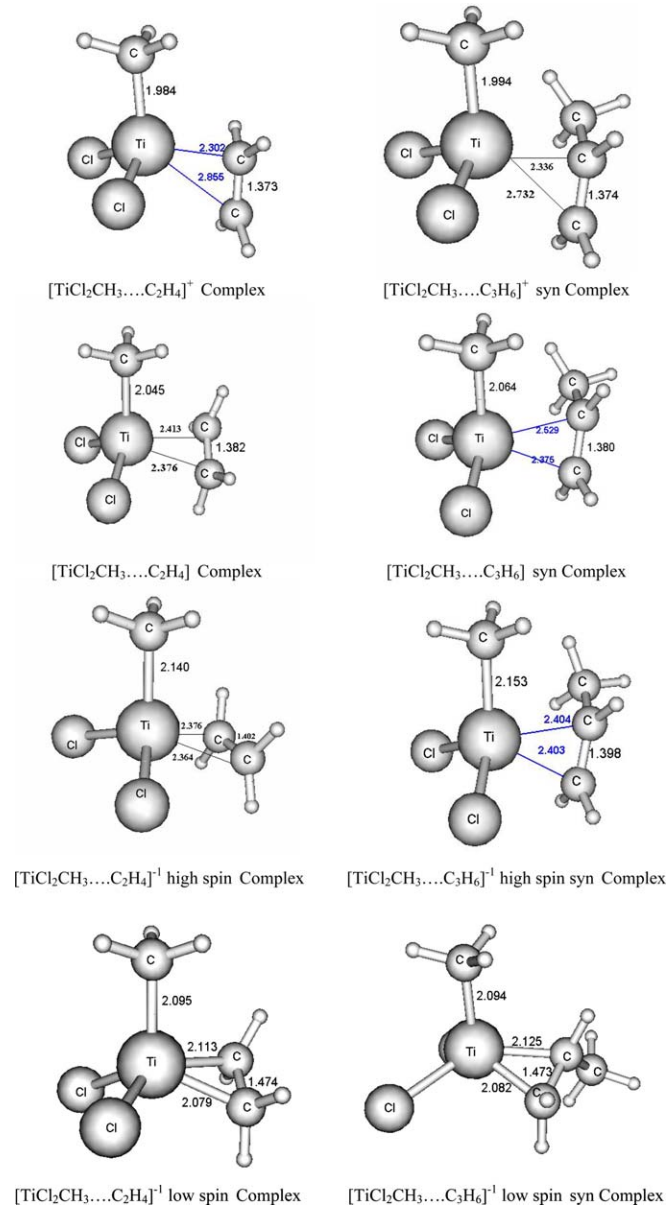

Fig. 2. Optimized geometries of all ethylene and propylene complexes of $[TiCl_2CH_3]^n$ ($n = +1, 0, -1$) active catalysts at B3LYP/LANL2DZ level. Bond lengths are in Å.

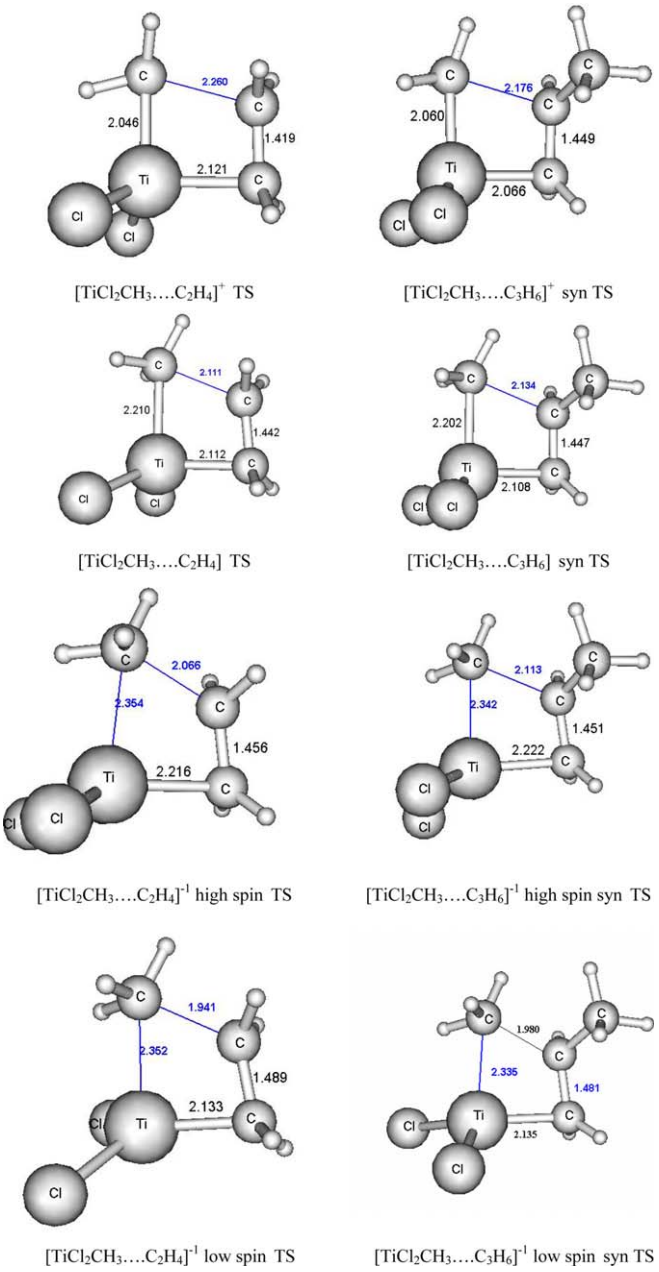

Fig. 3. Optimized geometries of all ethylene and propylene transition states of $[TiCl_2CH_3]^n$ ($n = +1, 0, -1$) active catalysts at B3LYP/LANL2DZ level. Bond lengths are in Å.

to reduction of radius from Ti(II) to Ti(IV) and stronger ability to accept electron density. Similar behaviour was previously observed in some Ti(III) and Ti(IV) systems [17a].

The structural aspects of the B3LYP/LANL2DZ optimized structures of active catalyst, olefin complexes, transition states and products of $[TiCl_2CH_3]^+$ with Ti(IV) oxidation state has already been dealt with in one of our previous works [4] and so will not be discussed in details here. Similar structural trends are also observed for these Ti(IV) systems even at extended B3LYP/LANL2DZ* level. The only exception to this is the geometry of *syn* propylene complex: At LANL2DZ level we found a *syn* complex with propylene parallel to Ti–CH_3 bond, however at LANL2DZ* similar complex has one small imaginary frequency ($-24.2\ cm^{-1}$) and a stable complex with olefin almost perpendicular to Ti–CH_3 bond was also found. Thus, we can assume that *syn* complex of propylene which has almost perpendicular geometry goes to an intermediate structure that is similar to *syn* complex geometry at LANL2DZ and subsequently undergoes propylene insertion into Ti–CH_3 bond.

In general, irrespective of oxidation states and the levels of calculation, some common trends are observed throughout the series: the elongation of C=C bond from free olefin to complexes and from complexes to corresponding

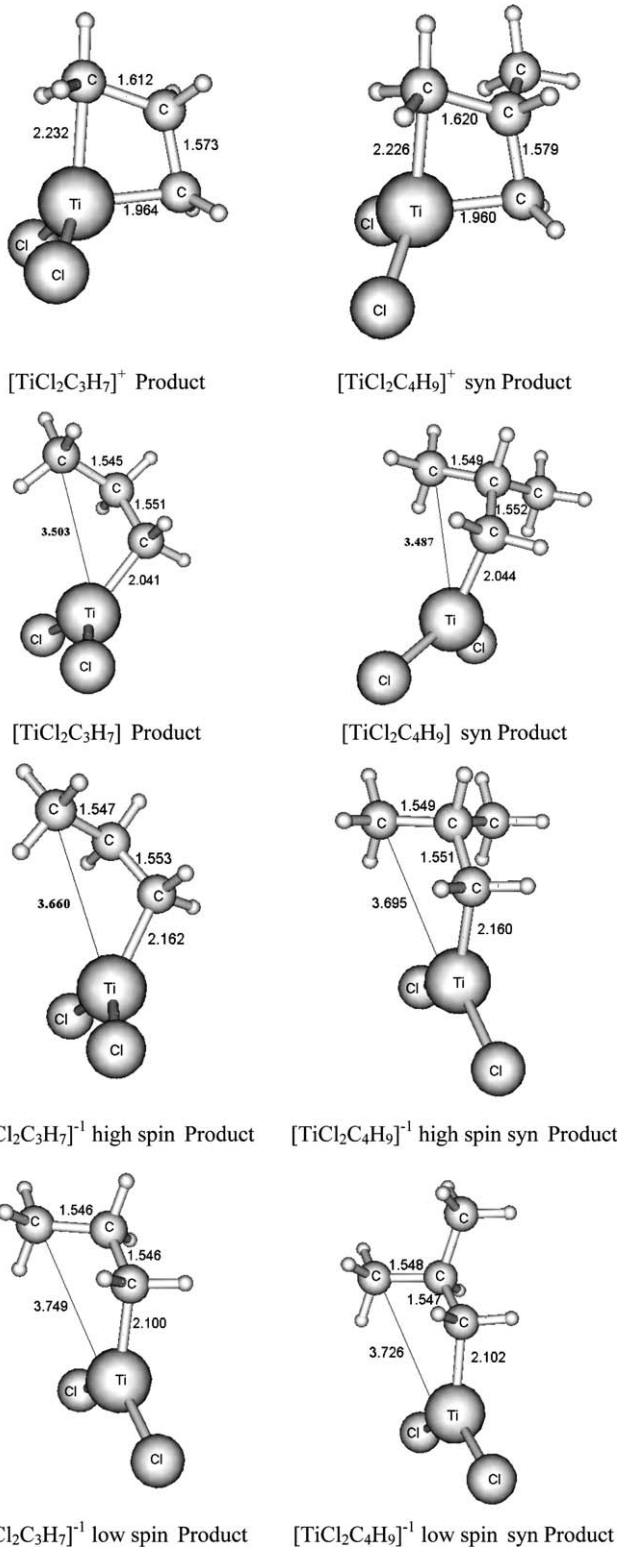

Fig. 4. Optimized geometries of all ethylene and propylene products of $[TiCl_2CH_3]^n$ ($n = +1, 0, -1$) active catalysts at B3LYP/LANL2DZ level. Bond lengths are in Å.

transition states (TSs), elongation of Ti–C(Me) and shortening of Ti–C(olefin) bonds from complexes to corresponding TSs are followed. Apart from the above trends, some notable differences on moving from the Ti(IV) to Ti(II) systems are: while the olefins are almost always in parallel orientation to the Ti–CH_3 bond in all complexes of the Ti(IV) system, they vary between parallel and perpendicular orientations to the Ti–CH_3 bond in the other Ti oxidation (cf. Table 2).

It is also interesting to note that while all the TSs for both ethylene and propylene Ti(IV) systems are early TSs (more *complex-like*), the TSs for both ethylene and propylene Ti(III) and Ti(II) high and low spin systems are late TSs (more *product-like*). This is reflected in the Ti–CH_3 elongation in the Ti(III) and Ti(II) high and low spin TSs compared to that in the Ti(IV) system (cf. Fig. 3). These TSs therefore lead to Ti(III), Ti(II) high and low spin products with growing alkyl chain that are more open and pointing away from Ti than the more closed product complexes of the Ti(IV) catalytic system with shorter Ti–C (terminal Me of growing alkyl chain) distances (cf. Fig. 4) with the terminal Me bending back closer to Ti. Such structural variation among the different Ti(IV) to Ti(II) transition states and products are reproduced at both LANL2DZ and LANL2DZ* levels. This is evident from the corresponding Ti–C (terminal Me of growing alkyl chain) distances in the olefin inserted products which change from 2.225–2.258 Å (2.204–2.243 Å) for Ti(IV) products to 3.487–3.674 Å (3.663–3.778 Å) for Ti(III) products to 3.068–3.694 Å (3.607–3.744 Å) for Ti(II) high spin products to 3.634–3.749 Å (3.634–3.785 Å) for Ti(II) low spin products at B3LYP/LANL2DZ (cf. Fig. 4) and B3LYP/LANL2DZ* levels (values in parentheses) of computation. The corresponding variation of the Ti–C–C (growing alkyl chain) bond angle is observed from acute angle values of ~82–85° for Ti(IV) products to obtuse angles in products of other Ti oxidation states, viz. Ti(III) ~113–121°, Ti(II) high spin ~115–122° and Ti(II) low spin ~114–123° at B3LYP/LANL2DZ (cf. Fig. 4) and very similar values and trends at B3LYP/LANL2DZ* level of computation. This structural variation can be rationalized on the basis of Mulliken charges on Ti and C* (terminal C of the growing alkyl chain) in all the products.

The Mulliken charges calculated at both B3LYP/LANL2DZ, LANL2DZ* (values in parentheses) in Ti(IV) and C* atoms in the ethylene, *syn* and *anti* propylene products are within ranges of 0.696 to 0.907 (1.014 to 1.128) for Ti(IV) and −0.851 to −0.853 (−0.481 to −0.536) for C*. These values correspondingly get reduced to 0.607 to 0.674 (0.852 to 0.887) for Ti(III) and −0.612 to −0.634 (−0.215 to −0.236) for C*. On moving to the Ti(II) high and low spin olefin inserted products, further reduction of Mulliken charges on Ti occurs to 0.358 to 0.387 (0.566 to 0.674) for the Ti(II) high spin centre and to 0.198 to 0.219 (0.204 to 0.288) for the Ti(II) low spin centre. The charges on C* range from −0.627 to −0.655 (−0.237 to −0.247) and from −0.631 to −0.657 (−0.187 to −0.321) in the Ti(II) high and low spin products, respectively. At both levels of calculation, this variation of charge on Ti

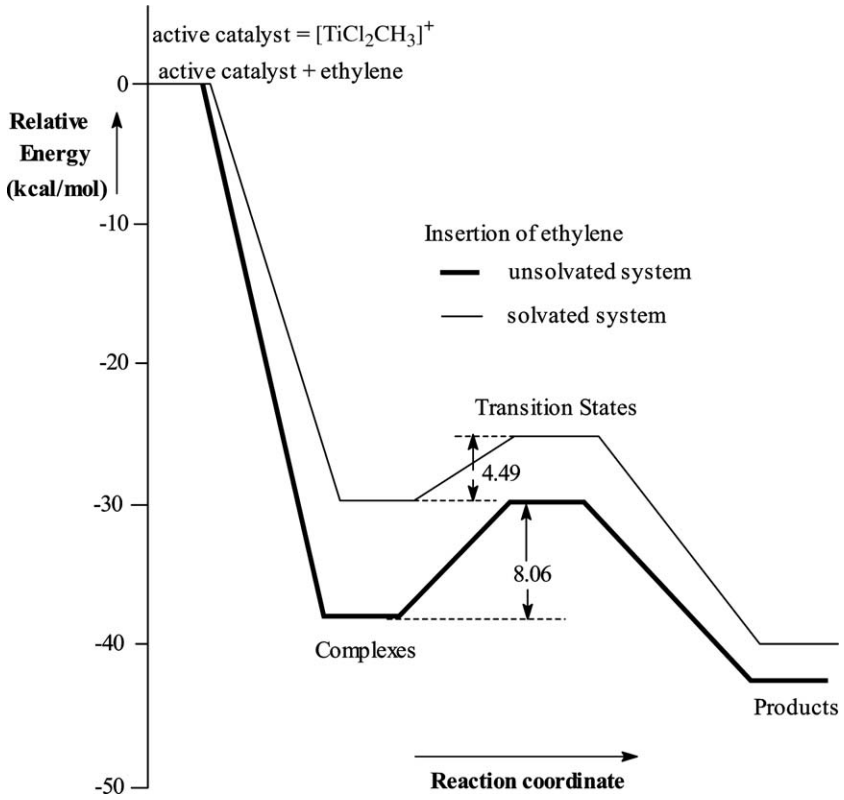

Fig. 5. Relative energy profile for ethylene insertion into solvated and unsolvated $[TiCl_2CH_3]^+$ at B3LYP/LANL2DZ level.

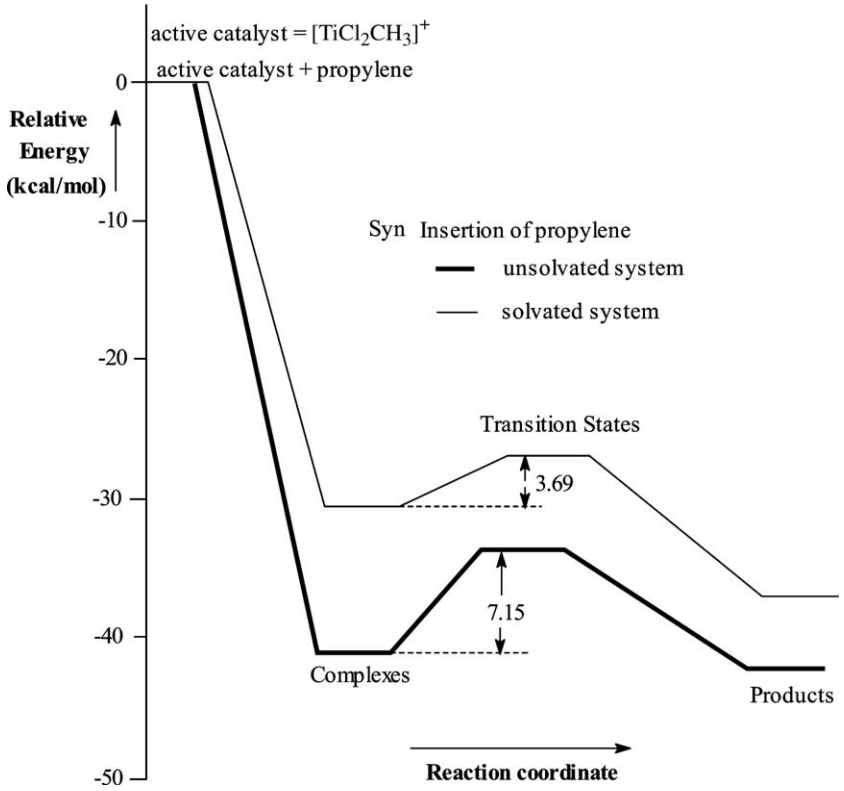

Fig. 6. Relative energy profile for propylene *syn* insertion into solvated and unsolvated $[TiCl_2CH_3]^+$ at B3LYP/LANL2DZ level.

clearly shows that the electrostatic attractive interactions between Ti centre and the terminal C of growing alkyl chain is maximum in the Ti(IV) products and progressively decreases in Ti(III) and Ti(II) products. This leads to Ti(IV) closed product structures with short Ti–C (terminal C atom of growing alkyl chain) distances having acute Ti–C–C (growing alkyl chain) angle. With decreasing Ti charge in other oxidation states, they exhibit longer Ti–C (terminal C atom of growing alkyl chain) distances and obtuse Ti–C–C angle leading to open product structures as shown representatively in Fig. 4 with B3LYP/LANL2DZ level structures.

In general, the agostic interactions observed also follow similar trends at both basis sets of calculation. We have earlier reported that for the Ti(IV) model system, the TSs for insertion of ethylene and propylene exhibit reasonable α-agostic interactions [4] and weak γ-agostic Ti···H(Me) interactions for the products. The agostic bond lengths reported below have been calculated at both B3LYP/LANL2DZ and B3LYP/LANL2DZ* (values in parentheses) levels showing similar trends.

In the Ti(IV) ethylene TS, the short Ti···H(CH_3) distance, 2.046 Å (1.983 Å) and one long C–H bond of CH_3, 1.140 Å (1.145 Å) against 1.096 Å, 1.091 Å (1.097 Å, 1.093 Å) for the other two C–H bonds is indicative of reasonable α-agostic interactions. In the corresponding Ti(IV) ethylene inserted product, the short Ti···H(CH_3) distance, 2.245 Å (2.112 Å) and one long C–H bond of CH_3, 1.116 Å (1.125 Å) against 1.114 Å, 1.094 Å (1.113 Å, 1.096 Å) for the other two C–H bonds is indicative of weak γ-agostic interactions.

These features however are not always found in all TSs and products of the other Ti oxidation states. For the Ti(III) and Ti(II) low spin ethylene TSs, all the Ti(II) high and low spin products and all the Ti(III) products no agostic interactions could be observed. Wherever present, the Ti(III), Ti(II) TSs have weak to very weak α-agostic interactions. Such agostic interactions lead to stabilization of the respective TSs.

Since similar trends of agostic interactions are observed for both levels of our calculations, we report here some representative agostics observed for the Ti(III) to Ti(II) TSs at B3LYP/LANL2DZ level (cf. Figs. 3 and 4). For the Ti(III) *syn* propylene TS, the short Ti···H(CH_3) distance, 2.351 Å and one long C–H bond of CH_3, 1.109 Å against 1.102 Å, 1.089 Å for the other two C–H bonds indicates very weak α-agostic interactions. For the Ti(III) *anti* propylene TS, the short Ti···H(CH_3) distance, 2.295 Å and one long C–H bond of CH_3, 1.111 Å against 1.090 Å, 1.099 Å for the other two C–H bonds indicates weak α-agostic interactions. For the Ti(II) high spin ethylene and *syn* and *anti* propylene TSs and for the Ti(II) low spin *syn* and *anti* propylene TSs, the short Ti···H(CH_3) distance ranges from around 2.300–2.400 Å and the corresponding C–H of CH_3 distances between 1.111 and 1.094 Å all indicating very weak α-agostic interactions.

3.2. Energetics

Ziegler et al. for their Ti(IV) and Ti(III) based constrained geometry catalysts (CGC) catalysts found that the much stronger Π-complex of Ti(III) is one the most important difference between Ti(III) and Ti(IV), which facilitate the subsequent insertion step [17a]. However, for the present model systems, we observe that Ti(IV) is more stabilized than Ti(III) complexes (cf. Table 1). In fact for our systems, at B3LYP/LANL2DZ level, the ethylene and *syn* propylene Π-complexation energies for the Ti(IV) system are around 38–41 kcal/mol which fall to about 12.4–12.6 kcal/mol for the corresponding Ti(III) systems (cf. Table 1) which agrees well with expected results since the reduction of Ti oxidation state and hence positive charge on Ti from IV to III also reduces the olefin-Ti interactions in Π-complexation. Similar relative energy results are also observed for our extended LANL2DZ* level calculations (cf. Table 1). These results markedly differ from those of Ziegler et al. for their Ti(IV), Ti(III) based CGC catalyst systems where the model considered itself is of a different system, CGC [(SiH2–C5H4–NH)TiCH3]^n ($n = 0$, +1), with ethylene binding energies of around 20.8 kcal/mol for the Ti(IV)- and around 22.7 kcal/mol for Ti(III)-based CGC system [17a].

We have found that the Π-complexation energies of ethylene with $[TiCl_2CH_3]^+$ containing Ti(IV) and with $[TiCl_2CH_3]^{-1}$ containing Ti(II) low spin, are comparable with values of −37.9 and −36.3 kcal/mol, respectively, and that for $[TiCl_2CH_3]$ with Ti(III) and $[TiCl_2CH_3]^{-1}$ with Ti(II) high spin are also comparable with values of −12.4 and −11.9 kcal/mol, respectively, at B3LYP/LANL2DZ level and similar relative energy values also at the extended LANL2DZ* level (cf. Table 1). This reflects that both Ti(IV) and Ti(II) low spin catalysts which are closed shell systems behave similarly in terms of ethylene complexation and the same is true for both Ti(III) and Ti(II) high spin catalysts which are open shell systems.

We have shown earlier that for Ti catalysts with different alkoxy and non-alkoxy ligands having varying heteroatoms (O, N, S), the insertion barriers for propylene are about 3–6 kcal/mol higher than the corresponding ethylene insertion barriers [4,5]. In contrast, in the present case, the activation barriers (E_{act}) for ethylene and propylene *syn* insertion in the Ti–CH_3 bond are comparable for different Ti oxidation states of +2, +3, +4. These are lower than corresponding barriers for propylene insertions in *anti* fashion at both levels of basis sets used (cf. Table 1) [4]. We have earlier observed similar trends of *syn* propylene insertion barriers being lower than *anti* barriers with the Ti(IV) catalyst system [4,5] in accordance with known experimental facts and several modeling studies [16a,16b,23]. Our computational results at both levels of calculation for all the Ti oxidation states are in accordance with the experimental observation [24] that both ethylene and propylene can be polymerized using this catalyst.

As discussed earlier, in case of insertion of propylene in *syn* fashion in Ti(IV) catalyst at B3LYP/LANL2DZ* level, we observed *syn* complex as well as *syn* intermediate that leads to propylene insertion. The relative energy profile for *syn* propylene insertion into unsolvated $[TiCl_2CH_3]^+$ at B3LYP/LANL2DZ* level is displayed in Fig. 7. The entire process of propylene insertion is viewed as follows. The *syn* propylene Π-complexation energy is −42.93 kcal/mol and in a small uphill process of 1.72 kcal/mol this *syn* propylene complex converts to the corresponding intermediate (cf. Fig. 7). This process is required for the propylene to reorient from perpendicular to parallel orientation to Ti–CH_3 for insertion. This intermediate is stabilized by −41.21 kcal/mol (cf. Table 1 and Fig. 7) and the propylene is oriented favorably for converting to the corresponding *syn* TS. This intermediate gets converted to the corresponding *syn* TS with activation barrier (E_{act}) of 8.56 kcal/mol (cf. Table 1 and Fig. 7) which ultimately leads to the corresponding products. Thus, it's once again observed that the activation barriers (E_{act}) for ethylene (5.73 kcal/mol) and propylene *syn* insertion in the Ti–CH_3 bond (8.56 kcal/mol) are comparable for Ti(IV) oxidation state even at the LANL2DZ* level of calculations (cf. Table 1).

The $[TiCl_2CH_3]^+$ with Ti(IV) has the lowest E_{act} (where E_{act} = activation barrier of olefin insertion in Ti–CH_3 bond) for both ethylene and propylene. E_{act} progressively increases in the order Ti(IV) < Ti(III) < Ti(II) high spin < Ti(II) low spin active catalysts for both levels of basis sets used in the calculations (cf. Table 1). This indicates that catalyst activity for olefin polymerization would be highest for the Ti(IV) systems and progressively decrease from Ti(IV) to Ti(III) to Ti(II) systems in accordance with known experimental facts and several other modeling studies [16a,16b,23]. These results are in line with studies by Boero et al. [16b,16c] considering the highly reactive Ti(IV) centre as the dominant catalytic species possessing high degree of stereoselectivity to select the appropriate propylene enantioface in the chain growth process. Although other possibilities of Ti oxidation states in any Ziegler–Natta heterogeneous system were not excluded [14,25], this choice was based on the recent extended X-ray absorption fine structure (EXAFS) experiments [16c,26]. These and our results, however, differ from those of Ziegler et al. for their Ti(IV) and Ti(III) based CGC catalysts with a different model system as mentioned earlier. By using DFT-MM methods these authors had reported that the ethylene insertion process for both Ti oxidation states was quite feasible with the Ti(IV) and Ti(III) complexes possessing modest comparable insertion barriers [17a].

For our model systems, a comparison of the frontier orbitals (highest occupied molecular orbital (HOMO) and lowest unoccupied molecular orbital (LUMO)) energies of the active catalysts with those of uncomplexed ethylene and propylene, reveals the extent of back bonding in the complexes. We observe that back bonding of electrons from Ti-active catalyst (filled Π orbitals, HOMO) to olefin (LUMO, i.e., $Π^*$ anti-bonding MO) progressively increases in the order Ti(IV) < Ti(III) < Ti(II high spin) < Ti(II low

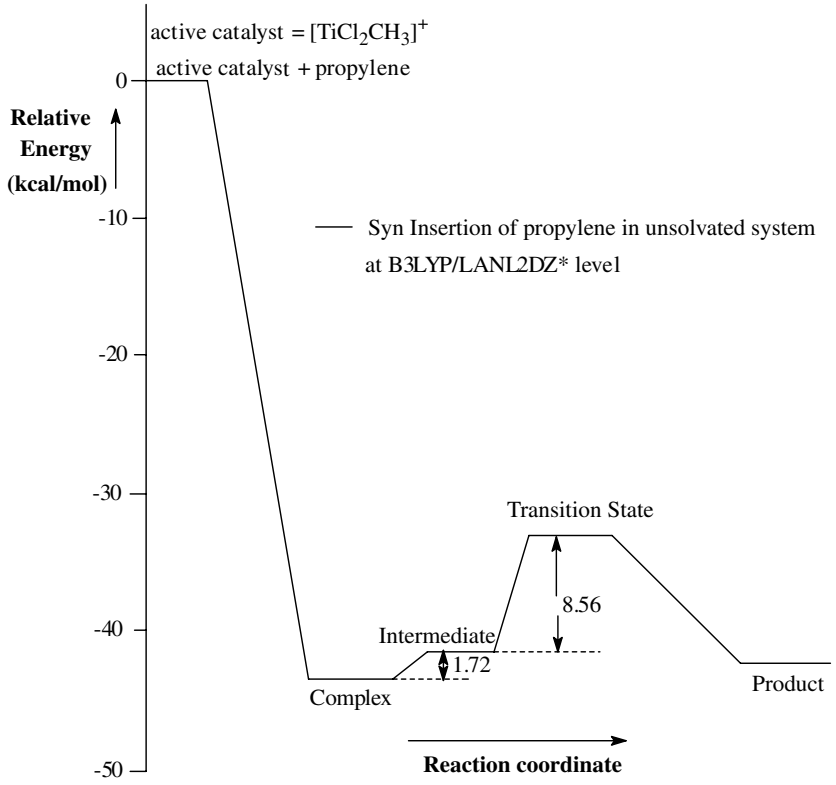

Fig. 7. Relative energy profile for propylene *syn* insertion into unsolvated $[TiCl_2CH_3]^+$ at B3LYP/LANL2DZ* level.

spin) catalyst systems with increased electron density on metal from Ti(IV) to Ti(II) for both B3LYP/LANL2DZ and LANL2DZ* level calculations (cf. Fig. 1). The extent of increase in electron density is also seen from decrease in charge on Ti for the Ti(II) systems over the Ti(III) and Ti(IV) systems (cf. Fig. 1). The effect of back bonding is also reflected in the corresponding C=C(olefin) elongation and Ti–C(olefin) shortening for both ethylene and propylene in the corresponding complexes across the series which is reproduced at both LANL2DZ and LANL2DZ* level of calculations (cf. Table 2). Such back bonding effects on C=C(olefin) and Ti–C(olefin) bond lengths have also been earlier reported by Ziegler et al. [17a] for ethylene insertion in Ti–CH_3 bonds of Ti(III) and Ti(IV) constrained geometry catalysts (CGC).

We have already observed that while the olefins are almost always in parallel orientation to the Ti–CH_3 bond in all complexes of the Ti(IV) system, they are in almost perpendicular orientations to the Ti–CH_3 bond in the Ti(II) complexes. This could be rationalized by the significant increase of Ti to olefin Π-back bonding on moving from Ti(IV) to Ti(II) systems. For Ti(IV) system, where the metal-olefin stabilizing interaction is mainly σ-donation from the olefin to Ti(IV), the Π orbital symmetry requirements are satisfied with parallel orientation of olefin with the Ti–CH_3 bond. In case of electron rich Ti(II) systems, the metal olefin stabilizing interaction is mainly due to back bonding from Ti (filled Π orbitals, HOMO) to olefin (Π*-antibonding LUMO) for which the appropriate orbital symmetries are satisfied with perpendicular orientation of olefin with respect to the Ti–CH_3 bond.

In order to study the effect of solvent in these systems, single point energy calculations on all the optimized geometries were carried out with toluene as solvent at B3LYP/LANL2DZ level using the CPCM method [20b]. A comparison of relative energies of the solvated systems with the unsolvated ones (cf. Table 1) reveals that in general some common trends are observed in both the solvated and unsolvated systems. The insertion barriers for ethylene and *syn* propylene are comparable, whereas propylene insertion in *anti* fashion has higher barriers for all oxidation states of Ti. The solvated Ti(IV) active catalyst has the lowest E_{act} over that for other Ti oxidation states. The order for E_{act} being Ti(IV) < Ti(III) < Ti(II) high spin < Ti(II) low spin for all the solvated catalysts. One of the notable differences between the two systems is that E_{act} for ethylene and *syn* propylene insertions get reduced to almost half the value in the solvated Ti(IV) system compared to that in the corresponding unsolvated system. There is no such dramatic change in the olefin insertion barriers for the Ti(III) and Ti(II) systems which show comparable insertion barriers both in solvated and corresponding unsolvated forms. The relative energy profiles for ethylene and *syn* propylene insertion into solvated and unsolvated $[TiCl_2CH_3]^+$ with Ti(IV) are displayed in Figs. 5 and 6, respectively. The relative energy profiles for the other Ti oxidation states are not shown since there is no appreciable change of olefin insertion barriers between unsolvated and solvated forms.

The effect of solvation for the Ti(IV) system is therefore twofold. Firstly, it destabilizes the solvated olefin complex with respect to the unsolvated analogues. Secondly, it destabilizes the corresponding solvated transition states with respect to the unsolvated analogues but to a much smaller extent. The net effect is a significant lowering of activation barrier for alkene insertion in the Ti(IV) system from unsolvated to solvated forms. In presence of solvent, in general Ti(II) and Ti(III) stationary points are stabilized over corresponding unsolvated states, however, the olefin insertion barriers remain more or less unchanged.

The net effect of solvation on olefin insertion barriers of our Ti(IV) catalyst system is therefore observed to be much more remarkable than its effect on the neutral Ti(III) and anionic Ti(II) catalyst systems.

4. Concluding remarks

It is well known that in the real Ti catalyzed Ziegler–Natta (ZN) polymerization, Ti exists in several oxidation states of +2, +3, +4 [15–17,23]. Our studies explored the effect of variation of these metal oxidation states on Ziegler–Natta catalyst activity in order to investigate which Ti oxidation states lead to most promising olefin polymerization activities.

The effect of forward- and back-bonding between metal and ligand on structure and catalyst activity of Ti(IV) to Ti(II) olefin complexes is explored and rationalized on the basis of orbital overlaps at B3LYP calculation levels of both LANL2DZ and its extended LANL2DZ* version. For both solvated as well as unsolvated $[TiCl_2CH_3]^n$ ($n = +1, 0, -1$) catalyst systems, we have found that: (i) The activation barriers (E_{act}) for ethylene and *syn* propylene insertion in Ti–CH_3 bond are comparable, and lower than corresponding barriers for *anti* propylene insertions. (ii) The $[TiCl_2CH_3]^+$ catalyst with Ti(IV) has the lowest E_{act} which progressively increases in the order Ti(IV) < Ti(III) < Ti(II) high spin < Ti(II) low spin catalysts. This indicates that catalyst activity for olefin polymerization would be highest for the Ti(IV) systems progressively decreasing from Ti(IV) to Ti(III) to Ti(II) systems as suggested in experimental and several other modeling studies [16a,16b,23]. All the above trends for the unsolvated Ti(IV) to Ti(II) systems are reproduced at both B3LYP/LANL2DZ and extended LANL2DZ (LANL2DZ*) levels of calculation. However, there is a remarkable decrease of ethylene and *syn* propylene insertion barriers to Ti–CH_3 bond only from the unsolvated Ti(IV) system to the solvated Ti(IV) system but not for the other Ti oxidation states as seen from the B3LYP/LANL2DZ level calculations on the solvated systems.

Our computational results for all the Ti oxidation states match well with the experimental observation that, in the real ZN system which is a mixture of +2, +3, +4 Ti oxidation states, both ethylene and propylene can be polymer-

ized using the conventional $TiCl_4/MgCl_2$ ZN catalyst. Finally, our computations unambiguously reveal that Ti(IV) is the most active species in Ziegler–Natta catalyst system although existence of other Ti oxidation states have been shown by several studies [14–17,23,25].

Acknowledgements

Authors are grateful to Professor S.R. Gadre, University of Pune, India and to Dr. Libero Bartolotti, East Carolina Supercomputing Center, USA for providing computer facility. Financial support for this work was provided by Reliance Industries Limited. We thank the referees for useful suggestions.

References

[1] T.J. Pullukat, R.E. Hoff, Catal. Rev. Sci. Eng. 41 (3–4) (1999) 389.
[2] R. Mulhaupt, in: G. Fink, R. Mulhaupt, H.H. Brintzinger (Eds.), Ziegler Catalysts, Springer, Berlin, 1995, p. 35, and references therein.
[3] E. Albizatti, U. Giannini, G. Morini, C.A. Smith, R. Zeigler, in: G. Fink, R. Mulhaupt, H.H. Brintzinger (Eds.), Ziegler Catalysts, Springer, Berlin, 1995, p. 413, and references therein.
[4] S. Bhaduri, S. Mukhopadhyay, S.A. Kulkarni, J. Organomet. Chem. 671 (2003) 101–112.
[5] S. Mukhopadhyay, S.A. Kulkarni, S. Bhaduri, J. Mol. Struct. (Theochem.) 673 (2004) 65–77.
[6] S. Mukhopadhyay, S.A. Kulkarni, S. Bhaduri, J. Organomet. Chem. 690 (2005) 1356–1365.
[7] N. Kashiwa, J. Yoshitake, Makromol. Chem. 185 (1984) 1781.
[8] C.W. Chien, S. Weber, Y. Hu, J. Polym. Sci. Part A 27 (1989) 149.
[9] D. Fregonese, S. Mortara, S. Bresadola, J. Mol. Catal. A 172 (1–2) (2001) 89.
[10] V.A. Zakharov, S.I. Makhtarulin, V.A. Poluboyarov, V.F. Anufrienko, Makromol. Chem. 185 (1984) 1781.
[11] Y.H. Huang, Q. Yu, S. Zhu, G.L. Rempel, L. Li, J. Polym. Sci. Part A 37 (1999) 1465.
[12] S.H. Kim, G.A. Somorjai, J. Phys. Chem. B 106 (2002) 1386–1391.
[13] S.H. Kim, G.A. Somorjai, J. Phys. Chem. B 104 (2000) 5519–5526.
[14] E. Magni, G.A. Somorjai, J. Phys. Chem. B 102 (1998) 8788–8795.
[15] G. Monaco, M. Toto, G. Guerra, P. Corradini, L. Cavallo, Macromolecules 33 (2000) 8953.
[16] (a) M. Boero, M. Parrinello, H. Weiss, S. Huffer, J. Phys. Chem. A 105 (2001) 5096–5105, and references therein;
(b) M. Boero, M. Parrinello, S. Huffer, H. Weiss, J. Am. Chem. Soc. 122 (2000) 501–509, and references therein;
(c) M. Boero, M. Parrinello, K. Terakura, J. Am. Chem. Soc. 120 (1998) 2746.
[17] (a) L. Fan, D. Harrison, T.K. Woo, T. Ziegler, Organometallics 14 (1995) 2018;
(b) M. Seth, P.M. Margl, T. Ziegler, Macromolecules 35 (2002) 7815–7829.
[18] (a) P. Cossee, J. Catal. 3 (1964) 65;
(b) E.J. Arlman, P. Cossee, J. Catal. 3 (1964) 80, 89, 99.
[19] (a) A.D. Becke, Phys. Rev. A 38 (1988) 3098;
(b) C. Lee, W. Yang, R.G. Parr, Phys. Rev. B 37 (1988) 785;
(c) A.D. Becke, J. Chem. Phys. 98 (1993) 5648.
[20] (a) C.E. Check, T.O. Faust, J.M. Bailey, B.J. Wright, T.M. Gilbert, L.S. Sunderlin, J. Phys. Chem. A 105 (2001) 8111–8116;
(b) V. Barone, M. Cossi, J. Phys. Chem. A 102 (1998) 1995–2001;
(c) S. Miertus, E. Scrocco, J. Tomasi, Chem. Phys. 55 (1981) 117;
(d) S. Miertus, J. Tomasi, Chem. Phys. 65 (1982) 239;
(e) M. Cossi, V. Barone, R. Cammi, J. Tomasi, Chem. Phys. Lett. 255 (1996) 327.
[21] M.J. Frisch, G.W. Trucks, H.B. Schlegel, G.E. Scuseria, M.A. Robb, J.R. Cheeseman, V.G. Zakrzewski, J.A. Montgomery Jr., R.E. Stratmann, J.C. Burant, S. Dapprich, J.M. Millam, A.D. Daniels, K.N. Kudin, M.C. Strain, O. Farkas, J. Tomasi, V. Barone, M. Cossi, R. Cammi, B. Mennucci, C. Pomelli, C. Adamo, S. Clifford, J. Ochterski, G.A. Petersson, P.Y. Ayala, Q. Cui, K. Morokuma, P. Salvador, J.J. Dannenberg, D.K. Malick, A.D. Rabuck, K. Raghavachari, J.B. Foresman, J. Cioslowski, J.V. Ortiz, A.G. Baboul, B.B. Stefanov, G. Liu, A. Liashenko, P. Piskorz, I. Komaromi, R. Gomperts, R.L. Martin, D.J. Fox, T. Keith, M.A. Al-Laham, C.Y. Peng, A. Nanayakkara, M. Challacombe, P.M.W. Gill, B. Johnson, W. Chen, M.W. Wong, J.L. Andres, C. Gonzalez, M. Head-Gordon, E.S. Replogle, J.A. Pople, GAUSSIAN 98, Revision A.11, Gaussian Inc., Pittsburgh, PA, 2001.
[22] V.C. Gibson, S.K. Spitzmesser, Chem. Rev. 103 (2003) 283–315, and references therein.
[23] E. Albizzati, U. Giannini, G. Balbontin, I. Camurati, J.C. Chadwick, T. Dall'occo, Y. Dubitsky, M. Galimberti, G. Morini, A. Maldotti, J. Polym. Sci. A: Polym. Chem. 35 (1997) 2645.
[24] (a) A.K. Rappe, W.M. Skiff, C.J. Casewit, Chem. Rev. 100 (2000) 1435–1456, and references therein;
(b) S.M. Pillai, M. Ravindranathan, S. Sivram, Chem. Rev. 86 (1986) 353;
(c) M.B. Welch, H.L. Hsieh, in: C. Vasile, R.B. Seymour (Eds.), Handbook of Polyolefins. Synthesis and Properties, Marcel Dekker, New York, 1993, pp. 21–37, and references therein;
(d) A. Parada, T. Rajmankina, J.J. Chirinos, A. Morillo, Eur. Polym. J. 38 (2002) 2093–2099;
(e) U. Zucchini, I. Cuffiani, G. Pennini, Macromol. Chem. Rapid Commun. 5 (1984) 567–571.
[25] T.I. Kora'nyi, E. Magni, G.A. Somorjai, Top. Catal. 7 (1999) 179.
[26] P.J.V. Jones, R.J. Oldman, in: W. Kaminsky, H. Sinn (Eds.), Transition Metals and Organometallics as Catalysts for Olefin Polymerization, Springer, Berlin, 1988, p. 223.
[27] MDS 2.0, Molecular Design Suite, VLife Sciences Technologies Pvt. Ltd., Pune, India, 2005.